

Electron Spin Resonance with Ultra-sensitive Calorimetry

Jie Zhang

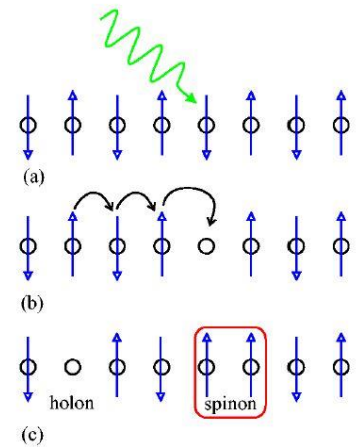
08/16/13

Outline

- Tomonaga-Luttinger Liquid
- Electron Spin Resonance (ESR) can be detected many ways
- ESR detection in Bulk CNTs (Bill's work)
- Setup details and properties

Tomonaga-Luttinger Liquid

- Fermi liquid----non-interacting free electron model (2D,3D);
- Tomonaga-Luttinger Liquid (TLL)----breaks down for 1D systems;



Some unique properties of TLL:

- Scaling law: Zero-temperature conductance $G = k \frac{e^2}{h}$, with universal constant k (observed but with controversy, hard to verify the universality and agreement with theoretical prediction);
- Transport measurement: the tunneling rate into a Luttinger liquid is suppressed to zero at low voltages and temperatures;
- Spin charge separation is one of the most interesting properties for TLL;

Tomonaga-Luttinger Liquid (continued)

- When $T \rightarrow 0$ K, electrons in solids can be considered as in one of three bound states: spinon (spin), orbiton (location), holon(charge);

$$H = H_{charge}(g_c) + H_{spin}(g_s)$$

- In TLL, H_c and H_s can be diagonalized independently,
and charge density mode with velocity v_c is not always

$$[H, H_c] = [H, H_s] = 0$$

equal to spin density mode with velocity v_s , $\begin{cases} \text{repulsive} & v_c < v_s \\ \text{attractive} & v_c > v_s \end{cases}$

- Physical systems believed to be described by the TLL model:

artificial quantum wires

electrons in carbon nanotubes

electrons moving along edge states in the fractional Quantum Hall Effect

electrons hopping along one-dimensional chains of molecules

fermionic atoms in quasi-one-dimensional atomic traps

a 1D chain' of half-odd-integer spins described by the Heisenberg model

Tomonaga-Luttinger Liquid Features observed in Ballistic SWNTs

- Measured nonequilibrium differential conductance and shot noise in ballistic SWNTs at low temperatures;
- Agreement with theory: reduced conductance oscillation amplitudes with increasing bias voltage and power-law characteristics in the weak backscattered current component;

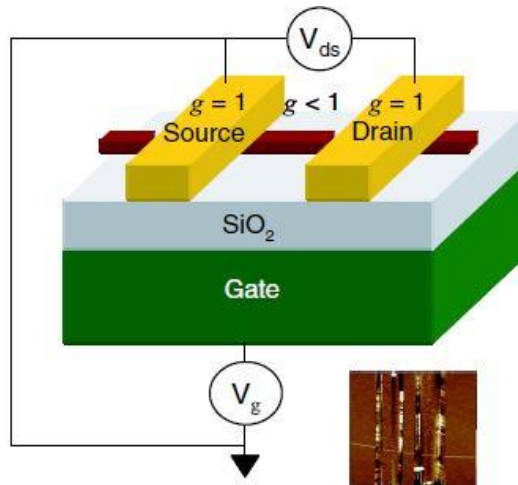


FIG. 1 (color online). Illustration of a three-terminal SWNT device with a interaction parameter g ($g = 1$ in the metal electrodes and $g < 1$ in the SWNT). Inset: atomic force microscope image of a device.

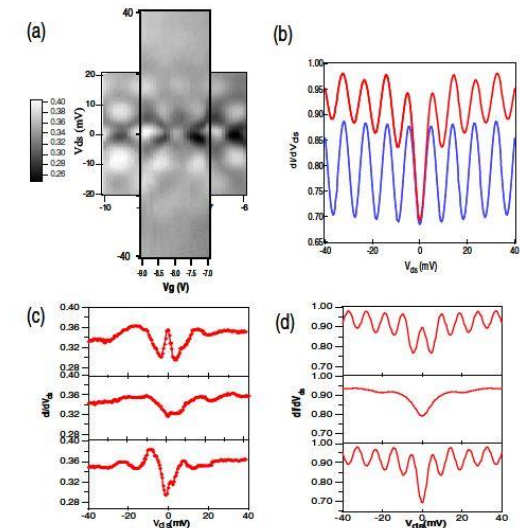


FIG. 2 (color online). Graphs of dI/dV_{ds} in units of $2G_Q$. (a) Density plot in V_{ds} and V_g . (b) Theoretical dI/dV_{ds} in V_{ds} at a given V_g for $g = 1$ (blue) and $g = 0.25$ (red) with $U_1 = 0.14$ and $U_2 = 0.1$ at $T = 4$ K. (c) Three experimental traces at $V_g = -9$ V (top), $V_g = -8.3$ V (middle), and $V_g = -7.7$ V (bottom). (d) Theoretical traces at $T = 4$ K for $U_2 = -0.1$ (top), $U_2 = 0$ (middle), and $U_2 = 0.1$ (bottom) with $U_1 = 0.14$.

ESR detection techniques

- Conventional method (commercialized): transmission spectroscopy---- measuring the absorption or transmission coefficient ;
- Magnetic torque detection: measuring the change that a magnetic resonance transition induces in the magnetization of the system;

$$\tau = M \times B$$

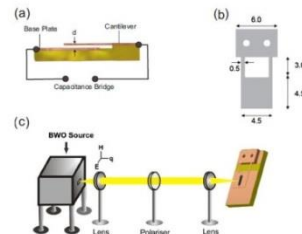


FIG. 1. (Color online) A drawing of (a) the torque meter with the cantilever placed at a distance d from the base plate, (b) the cantilever (all dimensions are in millimeter), and (c) the quasioptical setup which illustrates how the beam is focused onto the single crystal located on the cantilever.

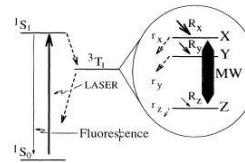
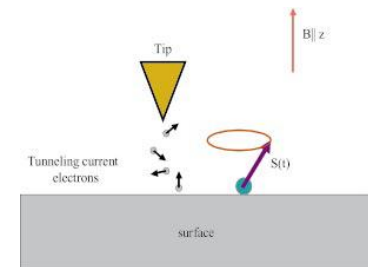


FIG. 1. Energy level scheme showing the singlet ground state 1S_0 , the first excited state 1S_1 , and the lowest excited triplet state 3T_1 . The energy separation of 1S_1 and 1S_0 is $\sim 16883 \text{ cm}^{-1}$; that of 3T_1 and 1S_0 is estimated to be $\sim 10000 \text{ cm}^{-1}$ [17]. Populating and depopulating rates of the triplet sublevels are denoted by $R_{X,Y,Z}$ with $R_X \sim 66 \text{ kHz}$, $R_Y \sim 29 \text{ kHz}$, $R_Z \sim 0.28 \text{ kHz}$, and $r_{X,Y,Z}$ with lifetimes $\tau_X, \tau_Y \sim 47 \text{ } \mu\text{s}$ and $\tau_Z^{-1} \sim 830 \text{ } \mu\text{s}$, respectively [10].



- Optically detected ESR;
- STM-ESR;
- Resistively detection: measuring the longitudinal resistance of 2DEG(Landau Level, Zeeman Splitting, filling factor);
- Thermal detection: measuring the temperature change induced by the non-radiative relaxation of the photon absorption;

How many spins at least can be detected?

- Ultimate goal in Spin Quantum Computation: addressing, manipulating and reading out individual spin;
- most sensitive induction-detection of ESR can detect 1000 spins:

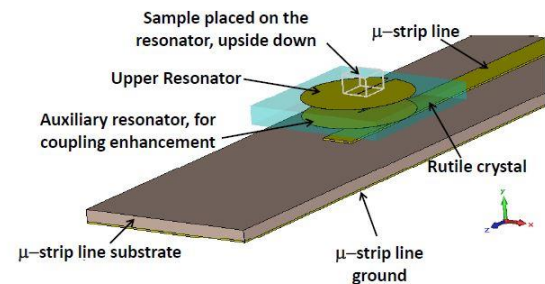
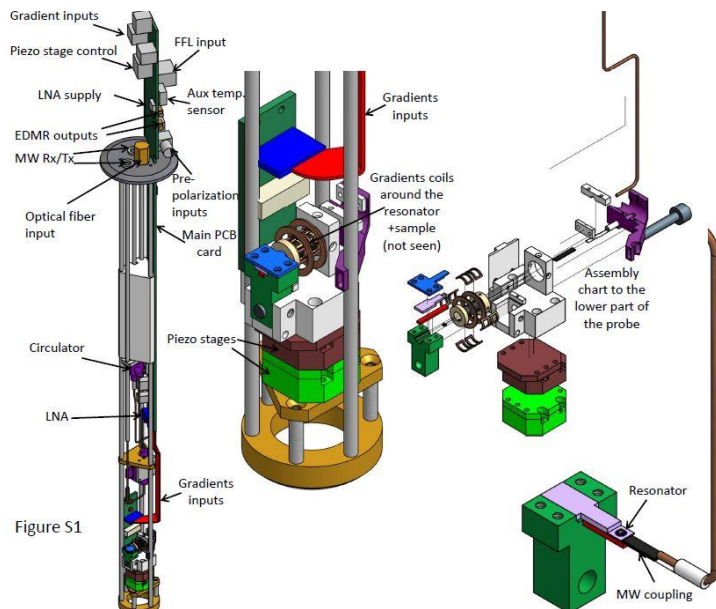


Figure S2

ESR in bulk SWCNTs

- Things to investigate: spin-orbit coupling, phase relaxation time, spin susceptibility and spin diffusion;
- ESR signal intensity increases after annealing and increases with decreasing temperature;

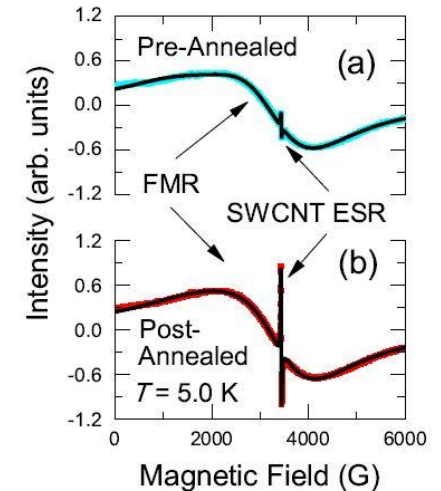
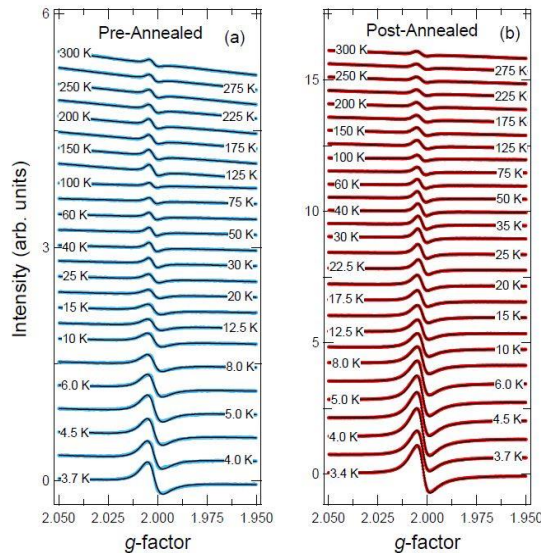


Figure 1: (a) Full range ESR scan at 5.0 K of SWCNT sample before annealing (cyan), where the ESR signal is buried in the large FMR background. (b) Full scan of SWCNT sample at 5.0 K after annealing (red), where the SWCNT ESR is the dominant feature. Black curves indicate fits composed of two large linewidth Lorentzian lines, which describe the FMR background, and a Dysonian line describing the SWCNT ESR. The FMR intensities stay the same before and after annealing.

- Relatively narrow linewidth corresponds to long decoherence time (~ 100 ns) ;

ESR in bulk SWCNTs (continued)

- Motional narrowing: ESR linewidth decreases as the temperature increase;

$$\Delta H = \Delta H_0 \exp\left(\frac{\Delta E}{k_B T}\right)$$
- Weak spin-orbit coupling make g factor $g = \frac{h\nu}{\mu_B H_0}$ approximately 2.

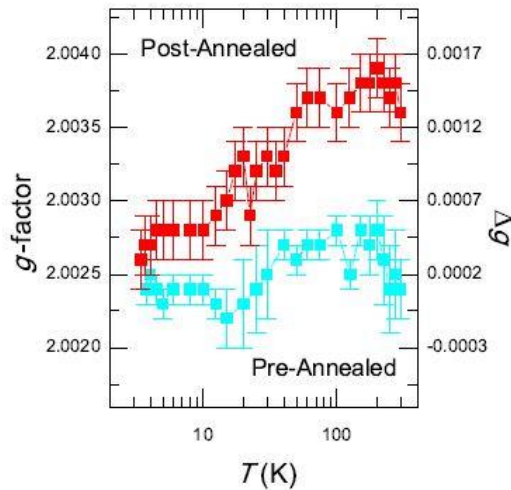


Figure 7: Experimentally obtained g -factor values as a function of T for the sample before (cyan) and after (red) annealing.

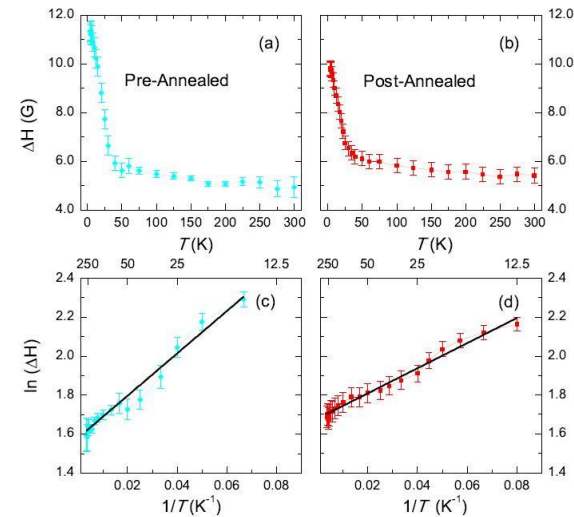


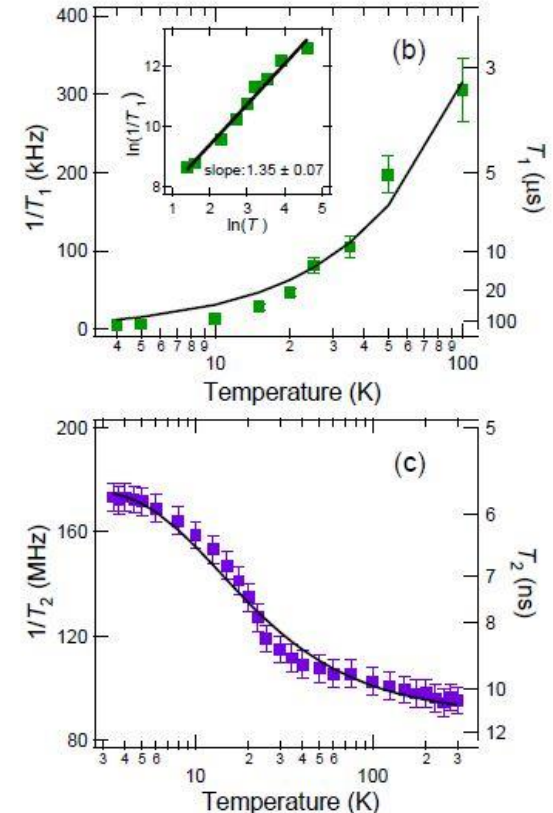
Figure 6: ESR linewidth versus T for the (a) pre-annealed and (b) post-annealed sample conditions. In (c) and (d), the natural logarithm of the data in (a) and (b) are plotted versus $1/T$ down to 15 K and 12.5 K, respectively. Black lines indicate linear fits to $\ln(\Delta H)$ versus $1/T$ data from which we can extract intertube hopping frequencies.

- Extracted χ_g from fitted spectra, the spin susceptibility follows a Curie-Law behavior:

$$\chi_g = C/T;$$

Spin-lattice relaxation time and spin-spin relaxation time

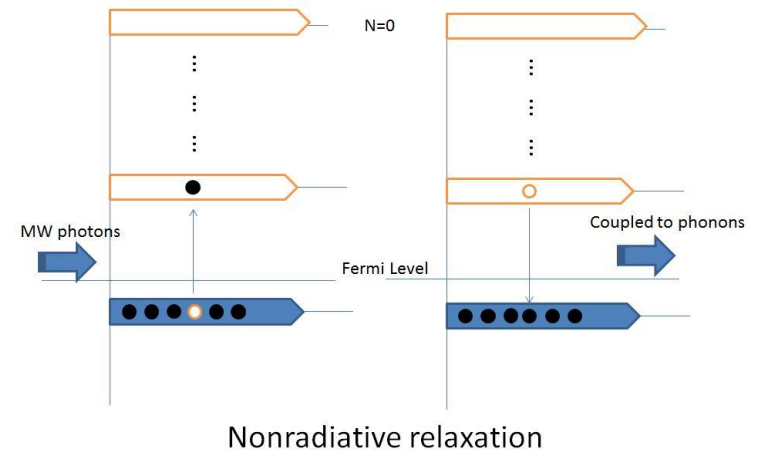
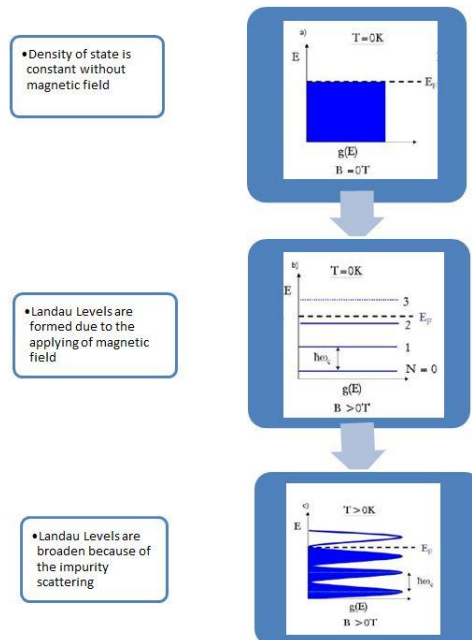
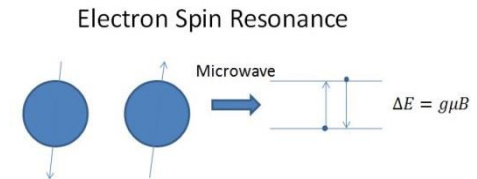
- Spin-lattice relaxation time T_1^{-1} is proportional to temperature => the probed spins relax through interaction with conduction electrons present in the metallic SWCNTs;
- G-factor difference from free electron value ($\Delta g = g - 2.0023$) suggests small spin-orbital coupling => direct spin-phonon coupling is small;
- Spin-spin relaxation time (dephasing rate) T_2^{-1} becomes smaller as T is increased due to motional narrowing;



Thermal detection of ESR (CR as demonstration)

Background:

- electrons coupled to phonons
- heat absorbed by lattice
- lattice temperature increased
- temperature detected by thermometer



Advantages over other methods

- Contacts not required;
- High sensitivity;

Where does the high sensitivity come from?

1. Sensitivity of the thermometer

Increases when temperature decreases;

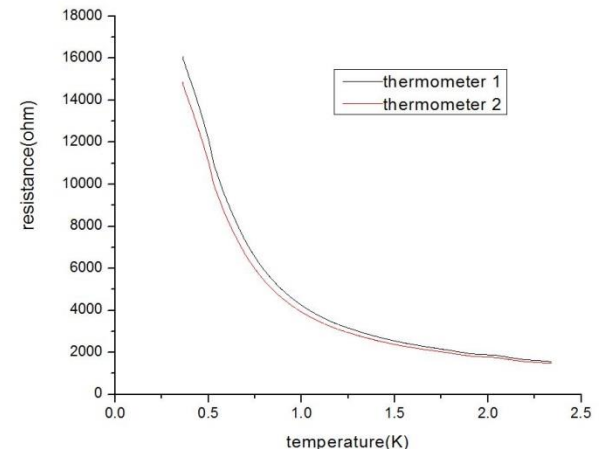
Use temperature as low as possible (300mK)

but with reasonable phonon coupling ;

2. Measuring techniques are employed

Differential method

Amplitude modulation



Sensitivity-----tens of **micro-Kelvin** temperature difference with **nano-watts** heating power

System and Construction

- He_3 Cryostat and coaxial cable probe
- 1266 epoxy vacuum can
- Sapphire crystal conduction bridge
- CX-1030 thermometer

Probe Schematics

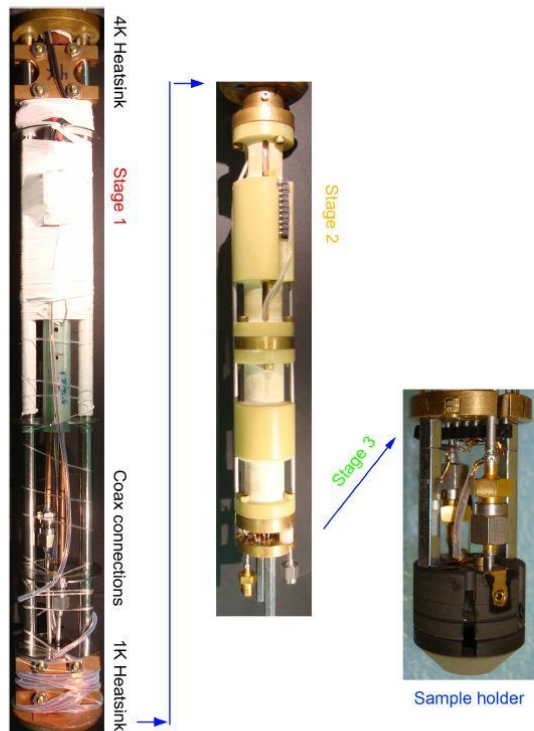
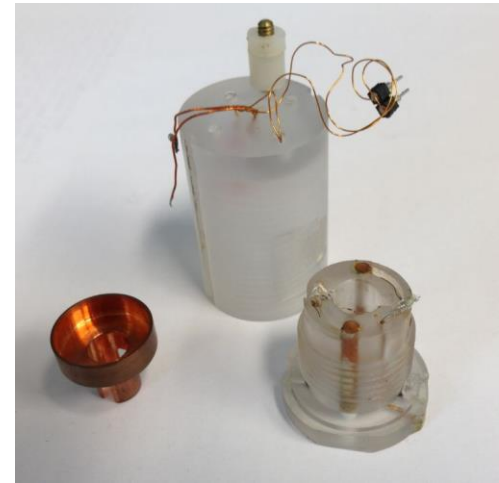


Figure D.1: Pictures of the probe stages: 4K, 1K, and the sample holder.



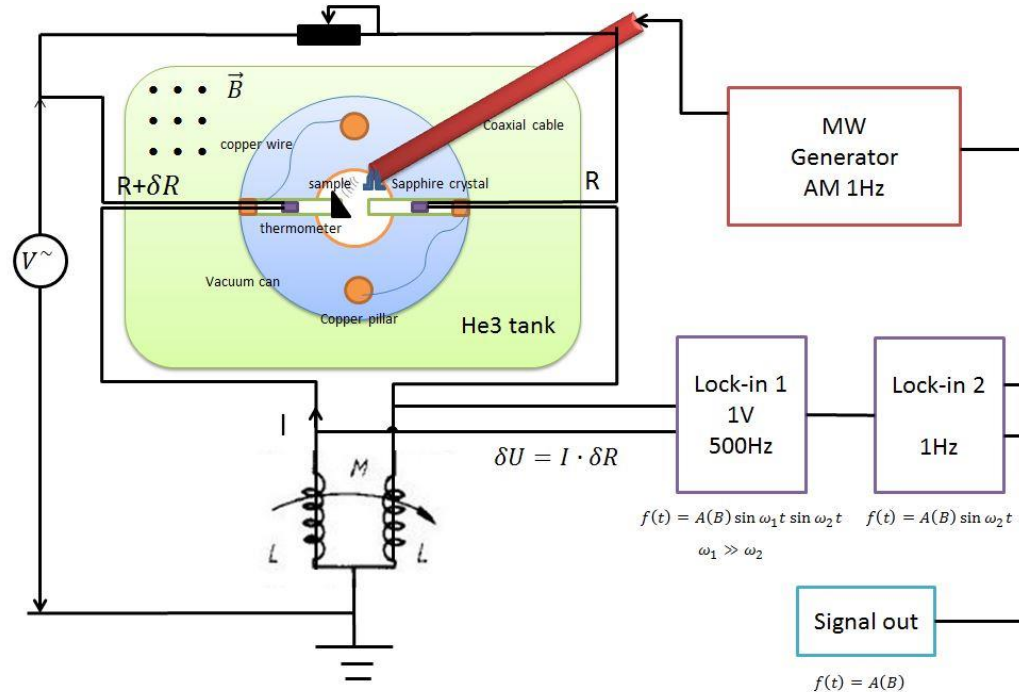
Measurement circuit

- Differential circuit
(to filter the background noise)

$$\frac{|\tilde{E}|}{|\tilde{V}|} = \left| \frac{\delta R \cdot j\omega_0(M+L)}{R^2 + 2R \cdot j\omega_0 L + \omega_0^2(M^2 - L^2)} \right| \approx \frac{\delta R}{2R}$$

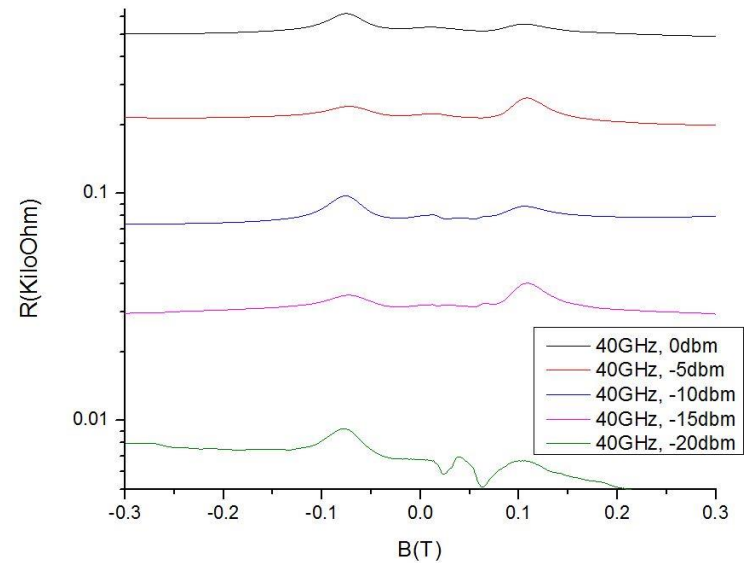
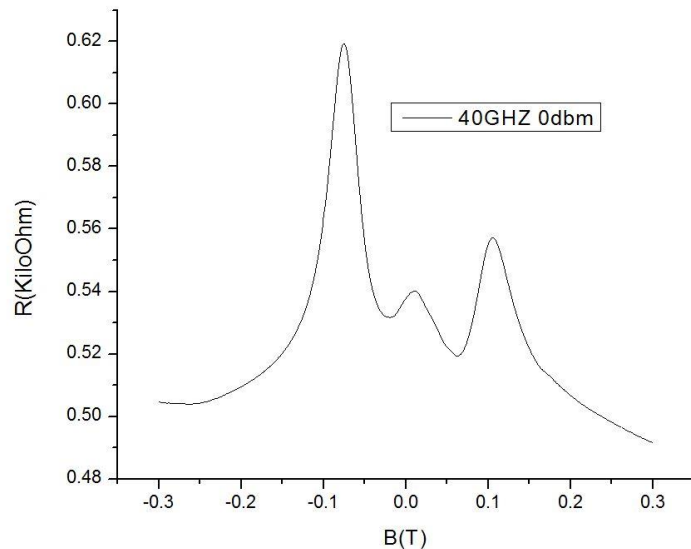
$$V_{out} \propto \delta R$$

- Amplitude modulation technique
(quench the asymmetry left in the differential geometry)



Experimental result

- Differential method is able to increase the sensitivity by roughly ten times while combined with amplitude modulation, another thirty times of sensitivity can be achieved.
- Even with microwave power as low as 0.01mW (-20dbm), signal can still be resolved.



Further work

- ESR of SWNTs;
- Reducing the sample size;

Reference

- [1] Direct observation of Tomonaga–Luttinger-liquid state in carbon nanotubes at low temperatures NATURE |VOL 426,2003
- [2] Tomonaga-Luttinger Liquid Features in Ballistic Single-Walled Carbon Nanotubes: Conductance and Shot Noise Kim, Recher, Oliver, Yamamoto
- [3] Torque detected broad band electron spin resonance REVIEW OF SCIENTIFIC INSTRUMENTS 81, 095105 2010
- [4] P. N. Murgatroyd and M. Belloufi, *A sensitive differential thermometer*. Meas. Sci. Technol. 1 (1990)
- [5] ESR-STM of a single precessing spin: Detection of exchange-based spin noise PRB 66, 195416 2002
- [6] Optically Detected Spin Coherence of Single Molecules PhysRevLett.71.3565
- [7] Enhancement of the Electron Spin Resonance of Single-Walled Carbon Nanotubes by Oxygen Removal William D. Rice
- [8] Spin relaxation times of single-wall carbon nanotubes PRB 88, 041401(R) (2013)
- [9] ESR-STM of a single precessing spin: Detection of exchange-based spin noise PRB 66, 195416 2002